Strain Gage Calibration of a Complex Wing

Jerald M. Jenkins,* Albert E. Kuhl,† and Alan L. Carter‡
NASA Dryden Flight Research Center, Edwards, Calif.

Modern, complex structural arrangements have complicated the task of measuring flight loads with calibrated strain gages. This paper examines the use of a relatively simple structural model to characterize the load responses of strain gages located on various spars of a delta wing. Strains measured during a laboratory load calibration of a wing structure are compared with calculations obtained from a simplified NASA structural analysis (NASTRAN) model. Calculated and measured influence coefficient plots that show the shear, bending, and torsion characteristics of typical strain-gage bridges are presented. Typical influence coefficient plots are shown for several load equations to illustrate the derivation of the equations from the component strain-gage bridges. A relatively simple structural model was found to be effective in predicting the general nature of strain distributions and influence coefficient plots. The analytical processes are shown to be an aid in obtaining a good load calibration. The analytical processes cannot, however, be used in lieu of an actual load calibration of an aircraft wing.

Nomenclature

b = wingspan
c = local wing chord
L = load (for example, shear, bending moment, or torsion)
x = distance from leading edge in chord direction
y = distance from chord in span direction
β = constant, Eq. (1)
$\bar{\beta}$ = average of equation constants
γ = shearing strain
δ = voltage change resulting from straining the active arms of a strain-gage bridge
δ_{cal} = reference voltage change resulting from shunting a calibrated resistor across one arm of a strain-gage bridge
ϵ = normal strain
η = nondimensional span notation, $2y/b$
μ = nondimensional strain-gage response, δ/δ_{cal}
ξ = nondimensional chord notation, x/c

Subscripts

$1,2,3...j$ = order of terms appearance in equation
i = discrete function

Introduction

CALIBRATED strain gages are commonly used to obtain flight loads data. They have most often been applied to high-aspect-ratio structures where structural redundancy is not great. When highly complex structures such as those used in some delta-wing supersonic aircraft are encountered, the usual approach has been to utilize pressure measurements to obtain the required loads data. This approach has been taken because of the uncertainties surrounding the application of conventional calibration philosophies[1] to the more sophisticated structural arrangements, such as those used for low-aspect-ratio supersonic configurations. Pressure measurements provide useful information; however, structural response cannot easily be measured from pressures. Certain types of information, such as structural response information, can be obtained most readily from calibrated strain gages.

Received Feb. 15, 1977; revision received June 29, 1977.
Index category: Testing, Flight and Ground.
*Chief, Aerostructures Division. Member AIAA.
†Staff Engineer, Aerostructures Division.
‡Deputy Chief, Aerostructures Division.

In the recent past,[2] the complex delta wing of a supersonic aircraft was successfully instrumented and calibrated for flight load measurements using strain gages. The purpose of this paper is to determine how well a relatively simple structural model can be used, before the fact, to identify and characterize the load responses of the strain gages located on various wing spars.

Background Information

The structural skeleton of half of a delta-wing aircraft is shown in Fig. 1. It is obvious that the multispar construction is highly redundant. Every other spar near the root of this wing was instrumented with strain-gage bridges. A load calibration of the structure was performed by applying discrete loads in a grid pattern over the surface of the wing.[2] The strain sensor outputs were recorded, and equations were developed from which surface loads could be determined.

The most common approach taken with calibrated strain gages does not involve using strain measurements directly. The load equations are most commonly developed from the electrical outputs of strain-gage bridges. The load equation generally takes the following form:

$$L = [\mu_1 \mu_2 \mu_3 \ldots \mu_j] \begin{Bmatrix} \beta_{11} \\ \beta_{12} \\ \beta_{13} \\ \cdot \\ \cdot \\ \cdot \\ \beta_{1j} \end{Bmatrix} \tag{1}$$

where L is the load, β is a constant, and μ is the nondimensional strain-gage response described as follows:

$$\mu = \delta/\delta_{cal} \tag{2}$$

In Eq. (2), δ is determined from the voltage changes of a strain-gage bridge, and δ_{cal} is a reference determined by shunting a calibrated resistor across one arm of the same strain-gage bridge.

Laboratory-measured strains, which are compared to the strains calculated from the structural model, are obtained

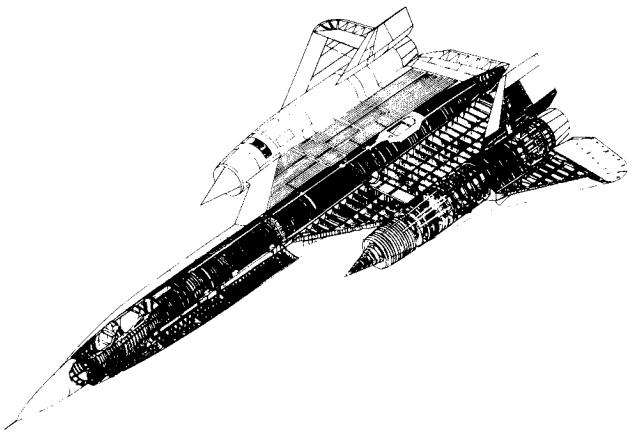

Fig. 1 YF-12 structural skeleton.

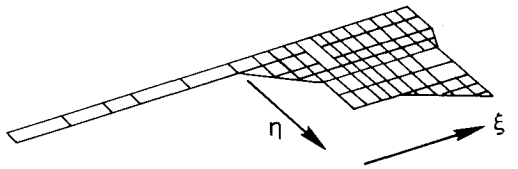

Fig. 2 Bar element NASTRAN structural model.

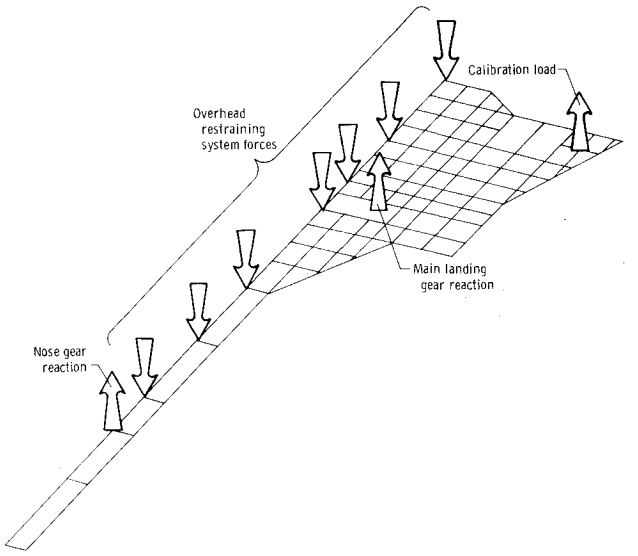

Fig. 3 Typical load condition.

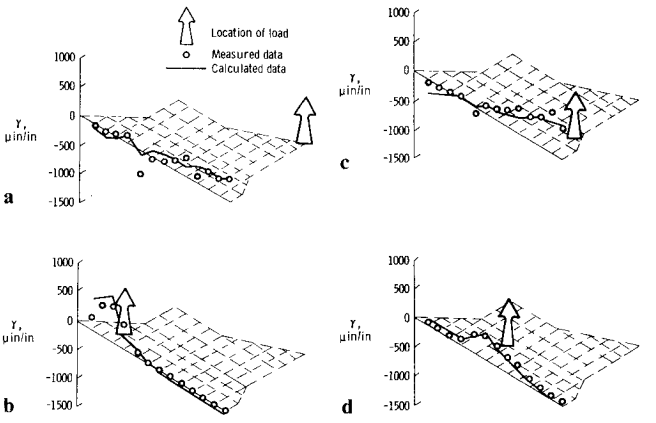

Fig. 4 Comparison of measured and calculated shear strains for several discrete loads.

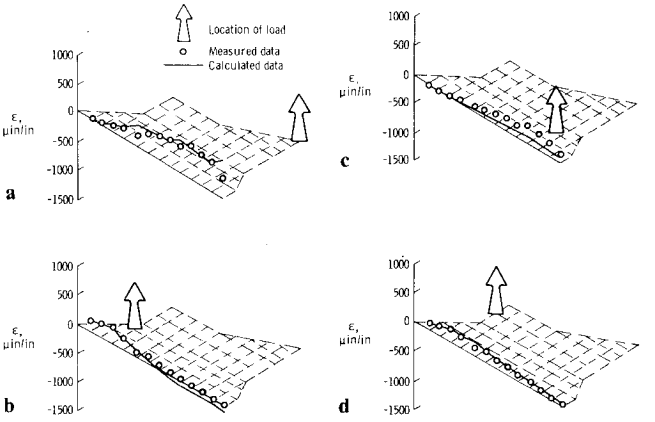

Fig. 5 Comparison of measured and calculated bending strains for several discrete loads.

from four active arm strain-gage bridges. This means that the test data at a discrete location when reduced to strains represent the average of the outputs of four strain gages located symmetrically with respect to the discrete location.

Structural Model

The delta-wing airplane described earlier was extensively instrumented and also extensively loaded in a laboratory, and a study was made of the resulting strain data. As part of the study, a simple NASA structural analysis (NASTRAN) model was created to provide predictive information.

A relatively simple model was chosen because it was economical and, thus, more realistic after the fact. The NASTRAN model of the structure is shown in Fig. 2. The model consisted of 102 node points and 178 bar (beam) elements. A typical laboratory load condition is shown in Fig. 3. An overhead restraining system was used to maintain a constant landing gear reaction for the different load conditions. The positions of the loads applied to the model were identical to those used in loading the actual airplane in the laboratory. This provided the basis for comparison.

To keep the number of bar (beam) elements small, the number of bar (beam) elements in the model used to represent the spars was half the actual number of spars. Each bar (beam) element spanwise in the wing represented the properties of the spar at that location plus one-half the properties of the adjacent spars. Each spar and rib combination was idealized as an upper and lower cap connected by a vertical shear web. The cap area was considered to be the sum of the actual spar cap and a portion of the cover skin. The amount of cover skin considered effective was determined from tests conducted by the manufacturer. The model beam inertias were computed from the magnitude and centroid location of these effective cap areas. Spanwise nacelle bending was represented by equivalent beams, which gave the same bending and shear stiffness as the actual nacelle rings.

The airplane wing beams are continuous across the fuselage for bending, whereas the wing shear loads are distributed to the fuselage rings through the wing root rib. The model's spanwise beams were carried into the centerline of the fuselage, and the fuselage itself was represented by longitudinal beams that simulated the bending stiffness of the fuselage shell and the shear stiffness of the wing root rib. The torsion stiffness of the wing was distributed to the spars and ribs (since there were no cover plates) by computing an equivalent polar moment of inertia for the model beams based on the torsion box area and the effective skin thickness. The torsion stiffness of the longitudinal beams representing the fuselage and nacelle was determined in a similar manner. The NASTRAN-calculated internal forces and moments were then

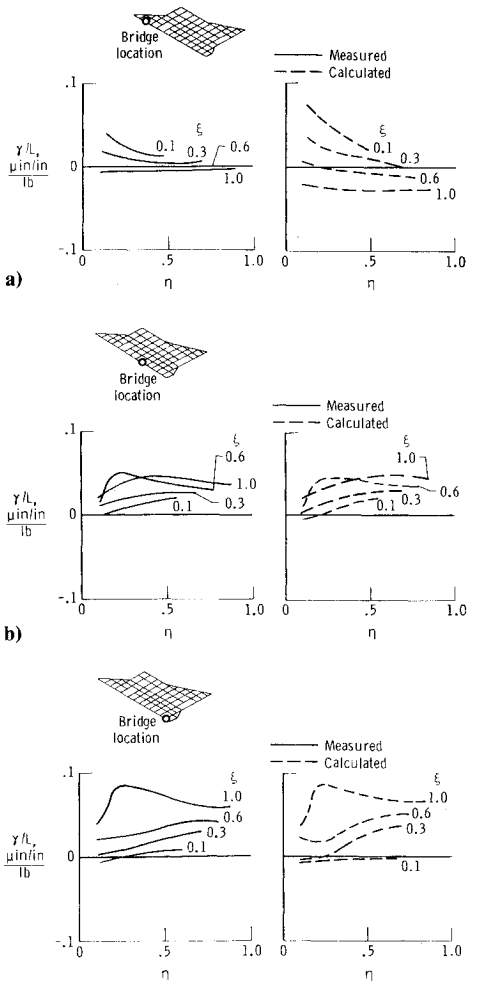

Fig. 6 Comparison of measured and calculated influence coefficient plots for shear strain.

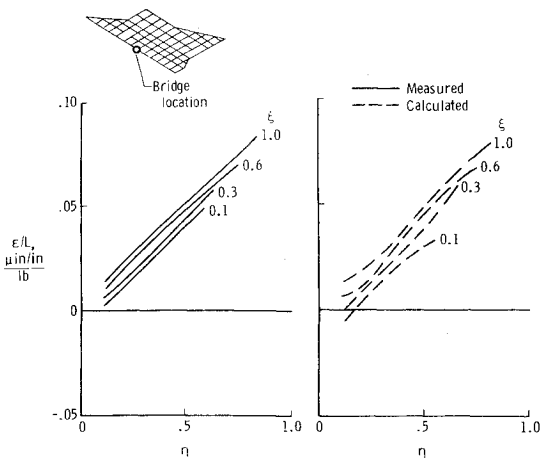

Fig. 7 Comparison of measured and calculated influence coefficient plots for bending strain.

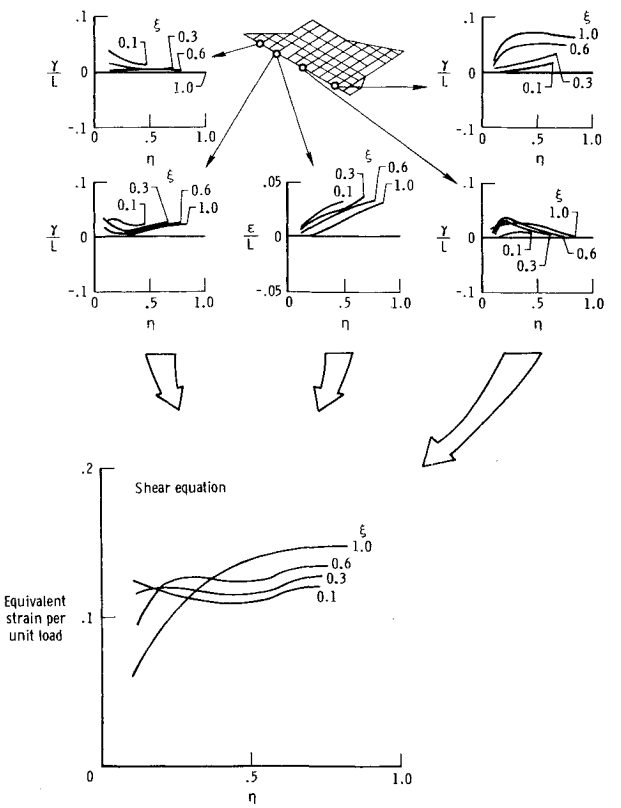

Fig. 8 Component experimental influence coefficient plots and corresponding load equation influence coefficient plot for typical shear equation.

distributed to the appropriate spars. Strains were calculated by using elementary theory.

Comparisons of Strains

Since the spars of the root section of the wing were instrumented to measure the strains due to the shear forces and bending moments caused by loads normal to the plane of the wing, the most fundamental comparison that can be made is the correlation of the calculated and measured strains.

Figure 4 compares shear strains measured in the laboratory and those calculated from the structural model for several load conditions. For these cases the model and the aircraft were restrained as shown in Fig. 3. The strain patterns at the root section vary considerably as the discrete load moves in the chord and span directions. The shifting of the strain pattern is especially apparent as the load moves from the leading edge to the trailing edge of the wing. This behavior, which is characteristic of multispar wings, is also reported in Ref. 3. When the load is near the leading edge of the wing (Fig. 4b), the spars near the trailing edge sense little strain. The converse is true when the load is near the trailing edge (Fig. 4c). It should be noted that the general agreement between the measured and predicted shearing strains is good. The strain responses at the root also shift as the load moves from outboard to inboard (Figs. 4a and 4d). This figure illustrates the effects of redundancy on the shear responses and the need for instrumentation on numerous spars to define the load responses over the entire surface of the wing.

A similar comparison is shown in Fig. 5 for bending strains. The chordwise effect observed with the shear strains is not nearly as pronounced. This is consistent with the fact that in general bending moments are easier to measure on an aircraft structure than shear or torsion loads.

Influence Coefficient Plots

Probably the most informative manner of presentation for load calibration data is the influence coefficient plot. The influence coefficient plot provides a way to look at the strain per unit applied load as a function of span for a given chord location for each strain-gage bridge. A plot of this nature is useful in determining whether a particular bridge is affected predominantly by shear, bending moment, or torsion loads, by a combination of two, or even by all three.

The influence coefficient plot of a single strain-gage bridge, such as the *i*th bridge, is the variation of the strain per unit load for loads at various span and chord locations, and can be

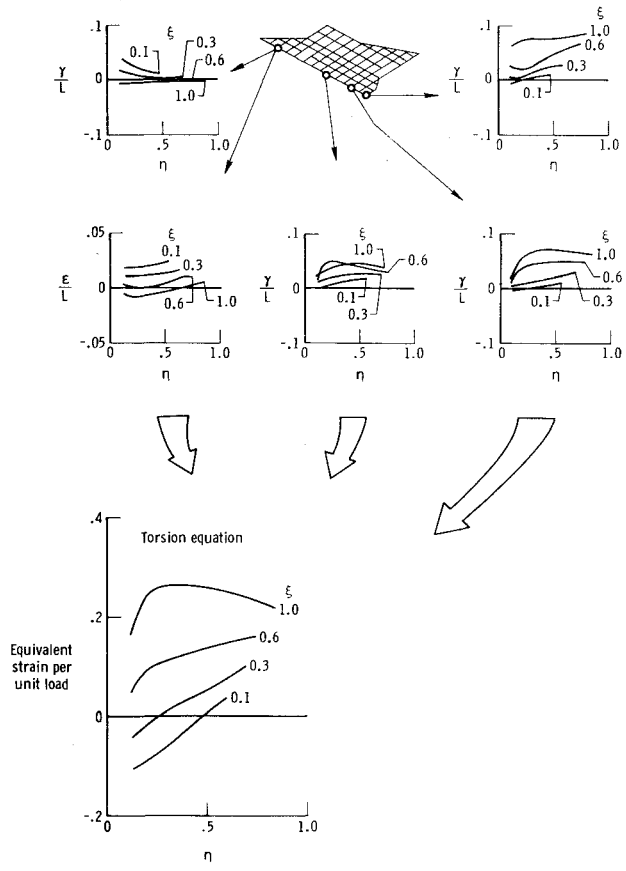

Fig. 9 Component experimental influence coefficient plots and corresponding load equation influence coefficient plot for typical torque equation.

expressed as follows:

$$\epsilon_i/L = f_i(\eta,\xi) \tag{3}$$

where ϵ_i is the strain at the ith bridge due to the applied load L, η is the nondimensional span location of the applied load ($\eta = 2y/b$), and ξ is the nondimensional chord location of the applied load ($\xi = x/c$).

Typical influence coefficient plots for shear strain are shown in Fig. 6. On the left are influence coefficient plots that were determined from the experimental load calibration. On the right are plots that were established from calculations using the NASTRAN structural model. Data for three shear bridges at locations varying from the leading to the trailing edge are presented. The character of the responses is predicted consistently; that is, the shapes of the curves and the positions of the curves with respect to each other are consistent. This was generally true at all strain-gage bridge locations. Occasionally, the measured output levels did not correlate with the calculations, as with the bridge located near the leading edge.

The influence coefficient plot of a typical bending bridge is shown in Fig. 7. In general, data from the bending bridges exhibited the same characteristics; the shapes of the predicted curves were close to those of the measured curves, with occasional discrepancies in the output levels.

Load Equations

It is revealing to compare influence coefficient plots of individual bridges with influence coefficient plots of complete load equations, which are developed from the combined information of the individual bridges. The influence coefficient plots for complete load equations are different from influence coefficient plots for individual strain-gage bridges.

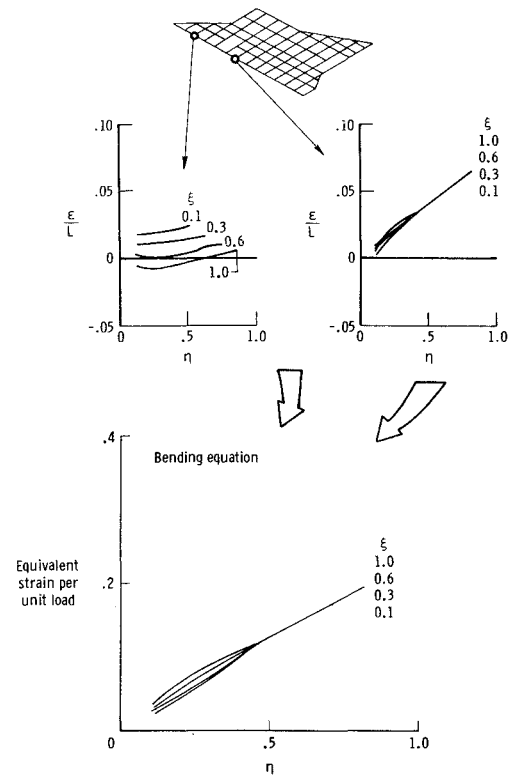

Fig. 10 Component experimental influence coefficient plots and corresponding load equation influence coefficient plot for typical bending equation.

The influence coefficient plot for a load equation, as presented in this paper, is the sum of the following terms:

$$\frac{\epsilon}{L} = \frac{\beta_1}{\bar{\beta}} f_1(\eta,\xi) + \frac{\beta_2}{\bar{\beta}} f_2(\eta,\xi) + \ldots + \frac{\beta_j}{\bar{\beta}} f_j(\eta,\xi) \tag{4}$$

where β_1, β_2, and so forth are the constants determined by the load equations, and $\bar{\beta}$ is the average of the constants of the equation. It is not necessary to divide by $\bar{\beta}$ to obtain a valid influence coefficient plot of the equation; division by $\bar{\beta}$ merely reduces the size of the multiplying numbers without altering the shape of the influence coefficient plot of the equation.

The influence coefficient plots of the individual bridges are used to form composite influence coefficient plots that represent complete load equations. As shown in Fig. 8, experimental data from five strain-gage bridges located on four different spars were used to formulate a load equation describing shear forces on the wing. The influence coefficient plot of the equation is shown at the bottom of the figure. The equation does not have a perfect shear response; a perfect shear expression would appear as a horizontal line, with all the chord lines falling on top of each other. However, bending and torsion effects have been greatly reduced.

A similar presentation of experimental data is made in Fig. 9. In this case, however, a torsion equation is presented. Once again, five strain-gage bridges located on four spars are used to formulate an equation that expresses the response to a discrete loading, which in this case is torsion. An ideal or perfect torsion equation would have an influence coefficient plot that possesses the same shape as the planform of constant chord lines. The equation is less than perfect; however, the improvement over the individual bridge characteristics is dramatic.

A bending equation obtained from experimental data is shown in Fig. 10. The strain-gage bridge at the top right exhibits an almost perfect bending response. A perfect bending response would be a straight, sloping line passing through the origin with all chord lines falling on top of each

other. An additional bridge at the top left was added to the equation to find out if it would improve the equation. The addition of this bridge to the equation improved the response of the bending bridge very little.

Concluding Remarks

A study was made to determine whether a relatively simple structural model of a complex delta wing would predict the response of the wing to load relatively accurately. It was found that the response of the wing to loads was generally predictable with a relatively simple model. The prediction of the character of the responses was accurate, although the prediction of the response's magnitude was less reliable. Influence coefficient plots predicted from a simple structural model may provide sufficient information to identify strain gages that may be eliminated and to select strain-gage combinations for use in load equations. The accuracy of the prediction also indicates whether the loading scheme covers all areas of the planform adequately and whether the locations of the strain gages on the structure are appropriate.

The relatively accurate prediction of influence coefficients does not, however, mean that an actual physical load calibration can be replaced by an analytical calculation. Instead, the analytical processes should be considered as only an aid in obtaining a good load calibration of an aircraft component. The illustration of this point has been the primary objective of this paper.

References

[1]Skopinski, T. H., Aiken, W. S. Jr., and Huston, W. B., "Calibration of Strain-Gage Installations in Aircraft Structures for the Measurement of Flight Loads," NACA Rept. 1178, 1954.

[2]Sefic, W. J. and Reardon, L. F., "Loads Calibration of the Airplane," *NASA YF-12 Flight Loads Program*, NASA TM X-3061, May 1974, pp. 61-107.

[3]Jenkins, J. M., Tang, M. H., and Pearson, G.P.E., "Vertical-Tail Loads and Control-Surface Hinge-Moment Measurements on the M2-F2 Lifting Body During Initial Subsonic Flight Tests," NASA TM X-1712, Dec. 1968.